Unique ATP-cone-driven allosteric regulation of ribonucleotide reductase via the radical-generating subunit

Inna Rozman Grinberg[1], Daniel Lundin[1], Mahmudul Hasan[1,2,#], Mikael Crona[3,#], Venkateswara Rao Jonna[4,#], Christoph Loderer[1], Margareta Sahlin[1], Natalia Markova[5], Ilya Borovok[6], Gustav Berggren[7], Anders Hofer[4], Derek T Logan[2,*] and Britt-Marie Sjöberg[1,*]

[1]Department of Biochemistry and Biophysics, Stockholm University, Sweden, [2]Department of Biochemistry and Structural Biology, Lund University, Sweden, [3]Swedish Orphan Biovitrum AB, Stockholm, Sweden, [4]Department of Medical Biochemistry and Biophysics, Umeå University, Sweden, [5]Malvern Instruments Inc., Sweden, [6]Department of Molecular Microbiology and Biotechnology, Tel-Aviv University, Israel, and [7]Department of Chemistry, Uppsala University. Sweden.

[#]These authors contributed equally

*Corresponding authors

Abstract

Ribonucleotide reductases (RNRs) are key enzymes in DNA synthesis and repair, with sophisticated allosteric mechanisms controlling both substrate specificity and overall activity. In RNRs, the activity master-switch, the ATP-cone, has been found exclusively in the catalytic subunit. In two class I RNR subclasses whose catalytic subunit lacks the ATP-cone, we discovered ATP-cones in the radical-generating subunit. The ATP-cone in the *Leewenhoekiella blandensis* radical-generating subunit regulates activity via modifications of quaternary structure induced by binding of nucleotides. ATP induces enzymatically competent dimers, whereas dATP induces non-productive tetramers, resulting in different holoenzyme complexes. The tetramer forms solely by interactions between ATP-cones, as evidenced by a 2.45 Å crystal structure. We also present evidence for an $Mn^{III}Mn^{IV}$ metal center. In summary, lack of an ATP-cone domain in the catalytic subunit was compensated by evolutionary capture of the domain by the radical-generating subunit. Our findings present a novel opportunity for dATP-regulation of engineered proteins.

Introduction

Allosteric regulation of an enzyme is defined as regulation of activity by binding of an effector molecule to a different location of the enzyme than the active site. The effector influences the distribution of tertiary or quaternary conformations of an enzyme, alone or in combination, modulating its activity (Swain & Gierasch, 2006). Allostery is an intrinsic property of many, if not all, dynamic proteins (Gunasekaran, Ma, & Nussinov, 2004) and an important factor in disease (Nussinov & Tsai, 2013), and has hence attracted considerable scientific interest. A substantial part of this interest has been focused on ribonucleotide reductase (RNR), which has been termed a “paradigm for allosteric regulation of enzymes” (Aravind, Wolf, & Koonin, 2000).

RNRs are essential enzymes in all free-living cells, providing the only known *de novo* pathway for the biosynthesis of deoxyribonucleotides (dNTPs), the immediate precursors for DNA synthesis and repair (Hofer, Crona, Logan, & Sjöberg, 2012; Nordlund & Reichard, 2006). To avoid misbalanced levels of dNTPs and the increased mutation rates that are the inevitable consequences of this (Kumar et al., 2011; Mathews, 2006; Watt, Buckland, Lujan, Kunkel, & Chabes, 2016), RNRs are tightly controlled through transcriptional and allosteric regulation, subcellular compartmentalization and small protein inhibitors (Pai & Kearsey, 2017; Torrents, 2014). Allosteric regulation of RNRs affects both substrate specificity and overall activity. The specificity regulation has been intensively studied and described for all three classes of RNRs (Andersson, Westman, Hofer, & Sjöberg, 2000; Hofer et al., 2012; Larsson et al., 2004; Reichard, 2010; Torrents et al., 2000; Zimanyi, Chen, Kang, Funk, & Drennan, 2016). The s-site binds dNTPs and determines which nucleotide will be reduced at the active site to ensure balanced levels of the four dNTPs in the cell. Additionally, many RNRs possess an overall activity regulation site (a-site) (Brown & Reichard, 1969; Thelander & Reichard, 1979) positioned in an N-terminal domain of ~100 amino acid residues called the ATP-cone (Aravind et al., 2000; Eriksson et al., 1997). Acting as a regulatory master switch, the a-site senses intracellular nucleotide concentrations by competitive binding of ATP and dATP. In presence of ATP the enzyme is active, and when concentrations of dNTPs rise, binding of dATP switches the enzyme off. This mechanism ensures sufficient but not excessive amounts of nucleotides that may also cause increased mutation rates (Mathews, 2006).

To date, ATP-cone domains in RNRs have been observed exclusively at the N-terminus of the catalytic subunit NrdA (class I), NrdJ (class II) and NrdD (class III). Class I RNRs consist of a large, catalytic subunit (α or NrdA), and a smaller, radical-generating subunit (β or NrdB) (Huang, Parker, & Stubbe, 2014; Nordlund & Reichard, 2006). NrdA and NrdB interact to form the active complex, in which the two proteins need to be precisely positioned such that the radical can be transferred from NrdB, where it is generated and stored, to NrdA where it starts the substrate reduction. In class I, it has long been noted that ATP-cones are absent from subclass Ib (NrdE) but present in several, but not all, NrdAs. A recent phylogenetic subclassification of RNRs reveals that three phylogenetically well-supported subclasses of class I never have ATP-cones (Jonna et al., 2015) (http://rnrdb.pfitmap.org): NrdE, NrdAi and NrdAk. In two of these subclasses we instead discovered ATP-cones attached to their corresponding radical-generating subunit: NrdF (the Ib subclass) and NrdBi. It hence appears as if the lack of activity regulation through an ATP-cone in the catalytic subunit is

compensated by the presence of this domain in the non-homologous radical-generating subunit of some RNRs.

Three distinct types of class I complexes have been mechanistically characterized and found to operate via nucleotide-induced regulation of quaternary structure (Johansson et al., 2016; Jonna et al., 2015; Kashlan, Scott, Lear, & Cooperman, 2002; Rofougaran, Crona, Vodnala, Sjöberg, & Hofer, 2008; Rofougaran, Vodnala, & Hofer, 2006; Torrents, Westman, Sahlin, & Sjöberg, 2006). Crystal structures, cryo-electron microscopy reconstructions and small-angle X-ray scattering studies of inhibited complexes have revealed that when dATP is bound at the a-site, high molecular mass oligomers are formed, in which the radical transfer pathway is distorted (Ando et al., 2011; Ando et al., 2016; Fairman et al., 2011; Johansson et al., 2016). Conversely, when ATP is bound, an active enzyme complex is formed. Interestingly, the structure and organization of subunits in active and inactive complexes varies considerably between species (Ahmad & Dealwis, 2013; Hofer et al., 2012). In *Escherichia coli* RNR, the active NrdAB complex is $\alpha_2\beta_2$, whereas the inactive form is an $\alpha_4\beta_4$ ring-shaped octamer where the ATP-cones in the α subunits interact with the β subunits (Ando et al., 2011). In the eukaryotic class I RNR, the inactive complex differs from *E. coli* in that it has an α_6 stoichiometry. This hexamer can only bind one β_2 subunit in an unproductive manner without a properly aligned electron transport chain (Fairman et al., 2011). Activation by ATP creates a different type of α_6 complex that binds one or more β_2 complexes (Ando et al., 2016; Aye & Stubbe, 2011; Crona et al., 2013; Fairman et al., 2011; Rofougaran et al., 2006). The different complexes are formed by subtle changes at the a-site induced by binding of the different nucleotides (Fairman et al., 2011). Another oligomerization mechanism has been recently found in *Pseudomonas aeruginosa* class I RNR, which possesses two consecutive ATP-cones, of which only the N-terminal one binds nucleotides. The active complex is once again $\alpha_2\beta_2$, but the inactive *P. aeruginosa* RNR complex is a dATP-induced α_4 complex consisting of a ring of four α subunits interacting via their outer ATP-cones (Johansson et al., 2016; Jonna et al., 2015). A single β_2 can bind to this ring, but the complex is inactive.

The unexpected finding of an ATP-cone fused to the radical-generating subunits poses questions regarding how it might regulate activity. Here we describe the mechanism of activity regulation by the ATP-cone N-terminally fused to the radical-generating NrdBi from *Leeuwenhoekiella blandensis* strain MED217. *L. blandensis* was isolated from Mediterranean surface seawater and belongs to Flavobacteriaceae, the major family of marine Bacteroidetes, with important roles in carbon flow and nutrient turnover in the sea during and following algal blooms (Fernandez-Gomez et al., 2013; Pinhassi et al., 2006). *L. blandensis* possesses two RNRs: a class II without ATP-cone, and the class I NrdAi/NrdBi, which lacks an ATP-cone in NrdA and instead contains an ATP-cone positioned at the N-terminus of NrdB. Superficially, the allosteric mechanism of *L. blandensis* NrdAi/NrdBi holoenzyme is similar to when the ATP-cone is contained in the catalytic subunit. At high dATP concentrations, inhibited higher oligomeric complexes of the holoenzyme are favoured. However, in the *L. blandensis* class I RNR, the oligomerization is driven by a shift towards tetramers of the radical-generating subunit. This illustrates how allosteric regulation controlled by ATP-cones can evolve in a highly dynamic way, requiring few adaptations to the core of the enzyme. The relative ease by which ATP-cone-driven activity regulation appears to evolve, provides a potential route to regulate engineered enzymes by dATP-inhibition.

Results

The activity allosteric regulatory ATP-cone is linked to the radical-containing subunit in some class I RNRs

We detected ATP-cones in the radical-generating subunits of RNRs from two distinct phylogenetic RNR subclasses: NrdBi and NrdF (Fig. 1a). In the NrdBi sequences, the ATP-cone was found at the N-terminus of the protein, whereas it was found at the C-terminus of the NrdF proteins (Fig. 1b). Interestingly, the corresponding catalytic subunit subclasses – NrdAi and NrdE respectively – have been found to lack ATP-cones. Ninety-three sequences in NCBI's RefSeq database are NrdBi proteins with N-terminally positioned ATP-cones. They are encoded by viruses and bacteria from several phyla, although the Flavobacteriales order in the Bacteroidetes phylum predominate (70 sequences, http://rnrdb.pfitmap.org). NrdF proteins with a C-terminally positioned ATP-cone are only encoded by four species of the Meiothermus genus of the Deinococcus-Thermus phylum (http://rnrdb.pfitmap.org). All species encoding NrdB proteins with ATP-cones in their genomes also encode other RNRs.

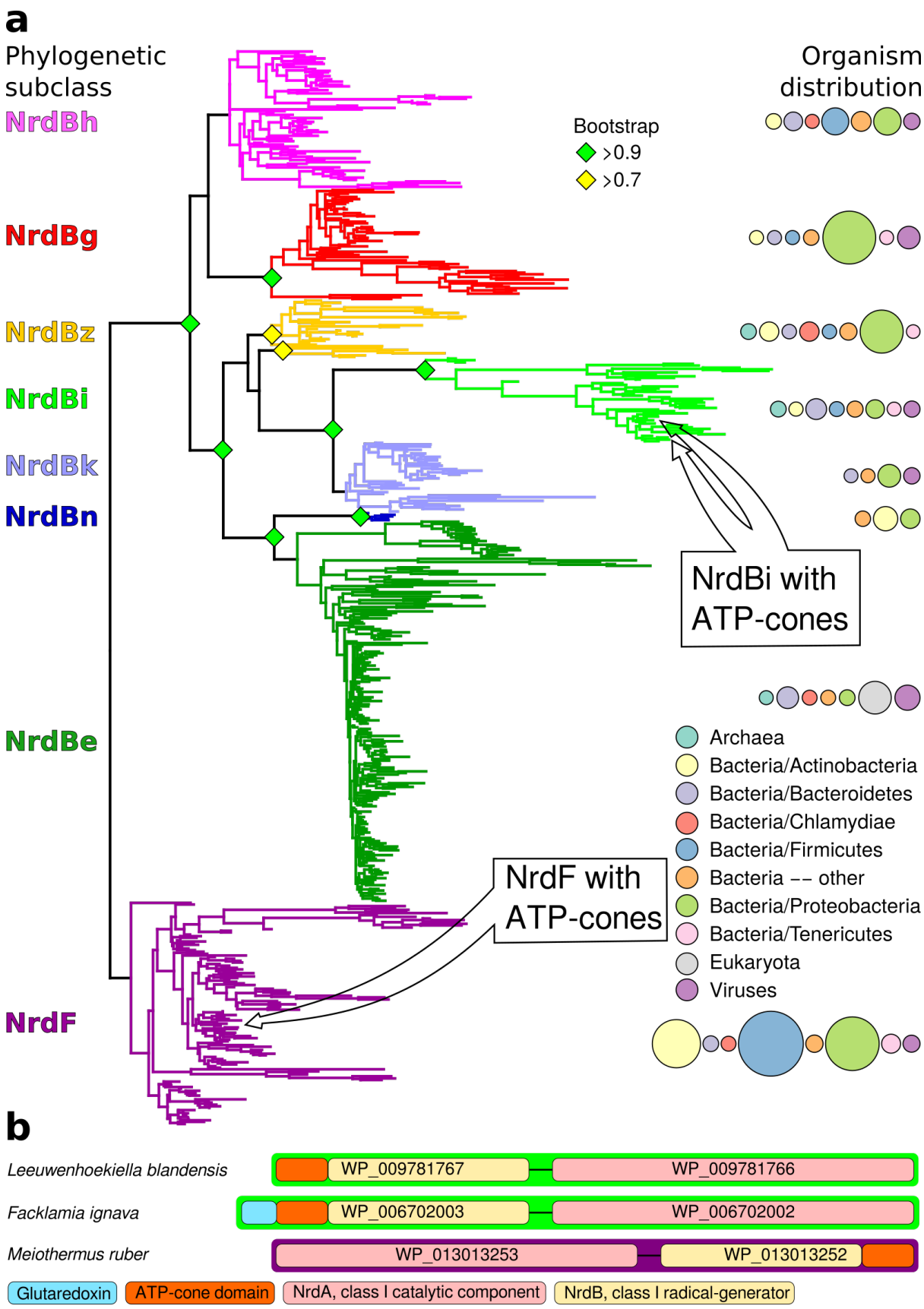

Figure 1. Unrooted phylogenetic tree of NrdB sequences and genome arrangements of NrdB sequences with ATP-cones. a) Maximum likelihood phylogeny of class I RNR radical generating subunit with subclasses in color, names to the left and organism

139 distributions to the right (see inset legend; sizes of circles are proportional to the number of
140 sequences found in each taxon). Bootstrap support values greater than 0.7 are shown with
141 colored diamonds. NrdBs with ATP-cones were discovered in two subclasses: NrdBi and
142 NrdF (formerly class Ib). Neither of the two subclasses have corresponding catalytic
143 subunits, NrdAi and NrdE respectively, with ATP-cones. In both subclasses, NrdB
144 sequences with ATP-cones were rare and phylogenetically limited, see inset arrows. b)
145 Arrangement of class I RNR genes in three genomes encoding NrdB proteins with ATP-
146 cones (*green borders*, NrdAi/NrdBi; *purple borders*, NrdE/NrdF). Genes are shown 5' to 3',
147 so that ATP-cones in the N-terminus are to the left in the gene.

148

149 Substrate specificity regulation of *L. blandensis* RNR via the s-
150 site

151 Initially we cloned, expressed and purified the *L. blandensis* NrdBi and NrdAi proteins. Using
152 a four-substrate activity assay in the presence of saturating concentrations of the s-site
153 effectors dTTP, dGTP or ATP, we found that *L. blandensis* RNR has a similar specificity
154 regulation pattern to most characterized RNRs (Hofer et al., 2012). ATP stimulated the
155 reduction of CDP and UDP, whereas dTTP stimulated the reduction of GDP, and dGTP
156 stimulated the reduction of ADP and GDP (Fig. 2). The enzyme was completely inactive in
157 the absence of allosteric effectors. Using mixtures of allosteric effectors, we observed that
158 dTTP-induced GDP reduction dramatically increased in the presence of ATP (Fig. 2).

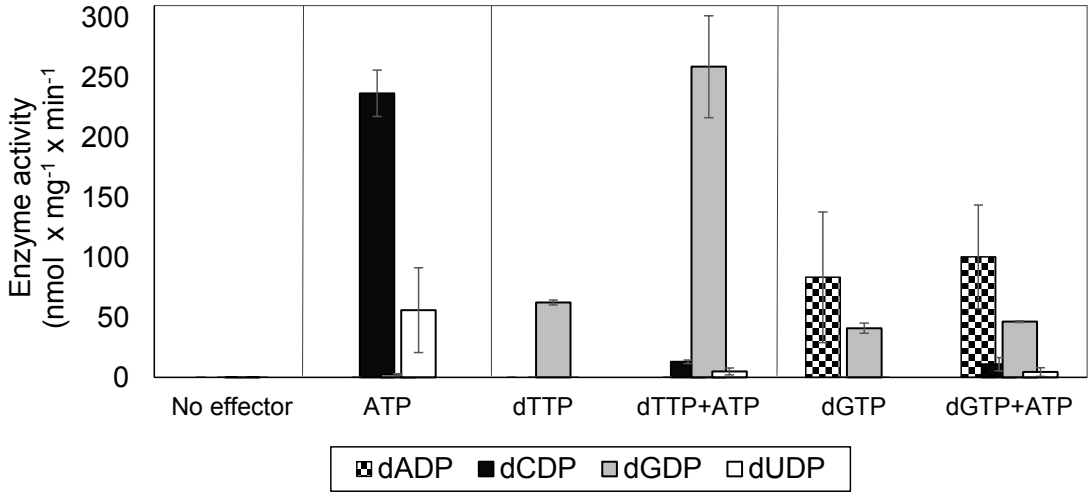

159

160 **Figure 2: Allosteric specificity regulation of the *L. blandensis* class I RNR.** Enzyme
161 activity was measured after 10 and 30 min in the presence of all four substrates (0.5 mM
162 each) and with the indicated allosteric effectors (2 mM of each). Error bars indicate the
163 extremes of two measurements. Protein concentrations were 1 μM NrdB and 4 μM NrdA.

164

165

Overall activity of *L. blandensis* RNR is regulated via the NrdB-linked ATP-cone

We performed a series of activity assays with CDP as substrate to elucidate the potential roles of ATP and dATP in activating and inhibiting the enzyme (Fig. 3). The presence of ATP clearly activated the enzyme (Fig. 3a), while dATP activated the enzyme when used at low concentrations and was inhibitory at 30 µM and higher (Fig. 3b). An ATP-cone deletion mutant NrdBΔ99, lacking the N-terminal 99 residues, reached a lower maximum activity compared to the wild type enzyme, suggesting that it was not activated by ATP beyond saturation of the s-site in the NrdA, nor was it inhibited by dATP (Fig. 3a-b). From the NrdBΔ99 effector titrations, we could calculate K_L values – the concentrations of allosteric effectors that give half maximal enzyme activity – for binding of ATP and dATP to the s-site in NrdA to 30 and 1.4 µM respectively. Titration of ATP into wild type NrdB in the presence of an excess of NrdA saturated with dTTP showed that it activates the enzyme through the a-site with a K_L of 96 µM (Fig. 3c). For the corresponding inhibition by dATP binding to the a-site, we calculated the K_i value - the binding constant of a non-competitive inhibitor - to be 20 µM in the presence of an s-site saturating dTTP concentration (Fig. 3d). We also tested if only the triphosphate form of (deoxy)adenosine nucleotides would interact with the a-site in presence of s-site saturating dTTP concentrations. In addition to ATP and dATP, dADP was also found to interact, whereas ADP, AMP and dAMP had no effect (Fig. 3e). Titration with dADP inhibited the enzyme activity, although less strongly than dATP (Fig. 3f).

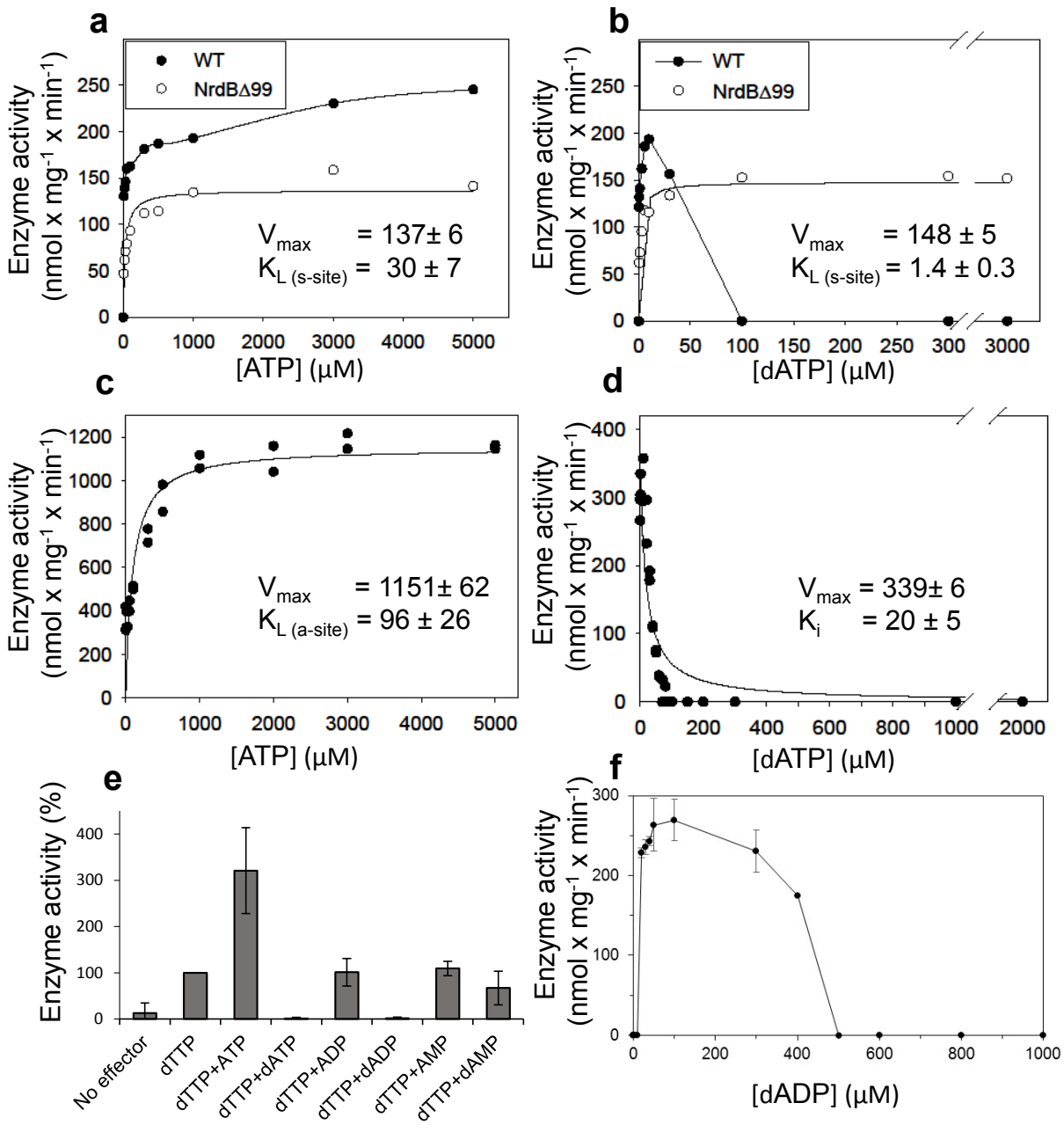

Figure 3: Activity of *L. blandensis* RNR with wild type NrdB or NrdBΔ99 in the presence of allosteric effectors. NrdB was used in excess over NrdA when studying the s-site and NrdA was used in excess when studying the a-site. a-b) CDP reduction assayed in mixtures of 0.5 μM NrdA and 2 μM of either wild type NrdB (black circles) or NrdBΔ99 (white circles), titrated with ATP (a) or dATP (b). c) GDP reduction assay mixtures with 2 μM NrdA and 0.5 μM wild type NrdB titrated with ATP in the presence of an s-site saturating concentration of dTTP (2 mM). d) Reduction of GDP assayed with 2 μM NrdA and 0.5 μM wild type NrdB, titrated with dATP in the presence of an s-site saturating concentration of dTTP (2 mM). e) GDP reduction in presence of s-site saturating dTTP (2 mM) and 2 mM of the indicated adenosine nucleotides. Assay mixtures contained 4 μM NrdA and 1 μM NrdB. 100% activity corresponded to 639 nmol x mg^{-1} x min^{-1}. f) CDP reduction assays titrated with dADP. Assay mixtures contained 2 μM NrdA and 0.5 μM NrdB. Error bars in panels E and F indicate the standard deviation of three measurements.

200

201 dATP binding to NrdB induces formation of higher oligomeric 202 complexes

203 To elucidate the mechanism of allosteric overall activity regulation governed by the NrdB-
204 linked ATP-cone, activity-independent oligomer-distribution experiments were performed by
205 gas-phase electrophoretic macromolecule analysis (GEMMA). In the absence of allosteric
206 effectors, NrdB (β) is mainly monomeric (theoretically 51.8 kDa) and in contrast to most
207 studied NrdB proteins it does not readily form dimers at the low protein concentration range
208 suitable for GEMMA analyses (Fig. 4a). Addition of dATP (50 μM) dramatically shifted the
209 equilibrium towards tetramers β_4, which became the major form under these conditions (Fig.
210 4a). Titration of increasing concentrations of dATP to NrdB showed that the tetramers
211 reached their half-maximum mass concentration at around 10 μM dATP (Supplementary Fig.
212 S1). Addition of 50 μM dADP also induced formation of NrdB tetramers (Fig. 4a). The
213 NrdBΔ99 mutant, lacking the ATP-cone (Fig. 4b), was in contrast mainly monomeric
214 regardless if dATP was present or not (Fig. 4b), demonstrating that the NrdB-linked ATP-
215 cone is required for dATP-induced tetramer formation. NrdA was a monomer (theoretically
216 70.6 kDa) in the absence of allosteric effectors, while addition of dATP prompted formation
217 of dimers (Fig. 4c) To assess the oligomeric state of the complete enzymatic complex of the
218 inactive *L. blandensis* RNR, a mixture of NrdA (α) and NrdB (β) in the presence of 100 μM
219 dATP was analyzed with GEMMA (Fig. 4c). The two subunits formed a large complex of 340
220 kDa with the expected mass of an $\alpha_2\beta_4$ complex (theoretically 348 kDa), and at higher
221 protein concentration a complex of 465 kDa with the expected mass of an $\alpha_4\beta_4$ complex
222 (theoretically 488 kDa).

223

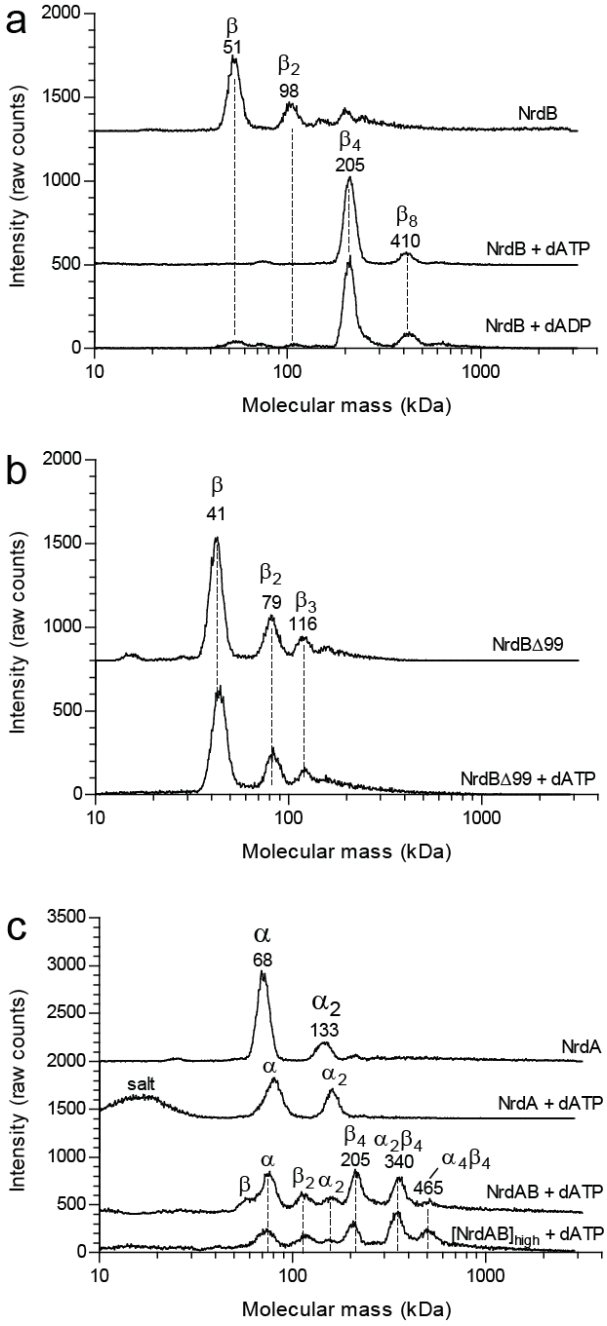

Figure 4: GEMMA analysis of the *L. blandensis* RNR subunits α, β and their combinations in the presence and the absence of allosteric effectors. a) 0.1 mg/ml NrdB (~2 μM) analyzed in the absence and presence of 50 μM dATP or dADP. b) The NrdBΔ99 mutant analyzed in the absence and the presence of 50 μM dATP. c) In the top two traces 0.1 mg/ml NrdA (~1.4 μM) is analyzed in the absence or presence of 100 μM dATP. In the third trace, 0.1 mg/ml NrdB is added to the mixture. The last trace is similar to the third trace, but the concentration of NrdA and NrdB is increased to 0.4 mg/ml NrdA and 0.3 mg/ml NrdB (~6 μM of each). The analyses of NrdA-NrdB complexes were performed at a very low pressure (1.4 Psi) to avoid the influence of magnesium-nucleotide clusters on the measurement and to minimize the risk of false protein-protein interactions. The baselines of the individual experiments are distributed in the vertical direction to be able to fit many traces in each panel.

To complement the GEMMA analyses of oligomer formation, we performed analytical size exclusion chromatography (SEC) using higher protein concentrations and physiologically reasonable concentrations of effectors (3 mM ATP and 0.1 to 0.5 mM dATP) (Bochner & Ames, 1982; Buckstein, He, & Rubin, 2008). At the higher protein concentrations used in SEC (as compared to GEMMA) NrdB eluted predominantly as dimers rather than monomers in the absence of effectors and similar results were also obtained in the presence of ATP. In agreement with the GEMMA results, the distribution was shifted towards tetramers in the presence of dATP (Fig. 5a). Without effectors, NrdA was mainly in a monomeric state, while it was dominated by dimers in the presence of either of the two effectors (Fig. 5b). When NrdA and NrdB were mixed in the absence of allosteric effectors, no complex was visible. After addition of ATP, a new complex of ~200 kDa appeared (Fig. 5c). To verify its composition and stoichiometry, we analyzed fractions eluted from SEC on SDS PAGE. Both NrdA and NrdB were visible on the gel in a 1:1 molar ratio (Fig. 5c insert). This complex, formed in conditions promoting active RNR, is conceivably an $\alpha_2\beta_2$ complex. After addition of the inhibiting effector dATP, a complex with a molecular mass consistent with $\alpha_4\beta_4$ eluted. The few differences between GEMMA and SEC are due to the different protein concentrations used and a complementary SEC study at lower protein concentration showed that the two methods are in good agreement with each other (Supplementary Fig. S2). A summary of the protein complexes formed in the presence and absence of effectors is presented in figure 5d.

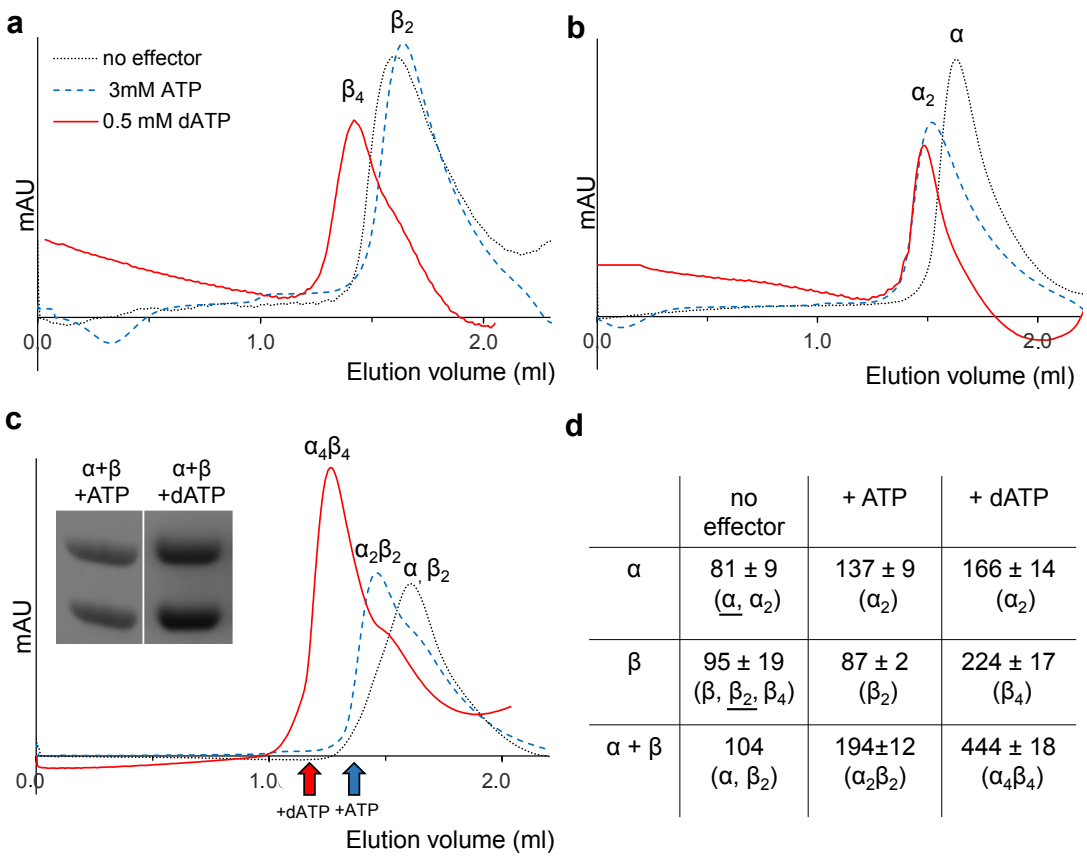

	no effector	+ ATP	+ dATP
α	81 ± 9 ($\underline{\alpha}$, α_2)	137 ± 9 (α_2)	166 ± 14 (α_2)
β	95 ± 19 (β, $\underline{\beta_2}$, β_4)	87 ± 2 (β_2)	224 ± 17 (β_4)
α + β	104 (α, β_2)	194±12 ($\alpha_2\beta_2$)	444 ± 18 ($\alpha_4\beta_4$)

Figure 5: Size exclusion chromatography of *L. blandensis* RNR in the absence and presence of 3 mM ATP or 0.5 mM dATP. Proteins at concentrations of 20 µM each were incubated separately or mixed together for 10 minutes in the absence (black dotted line) or presence of ATP (blue dashed line) or dATP (red solid line), centrifuged and applied to the column equilibrated with SEC buffer. Panels show NrdB (a), NrdA (b), and an equimolar mixture of NrdA and NrdB (c). C Insert: SDS PAGE of the eluted proteins run in the presence and absence of the indicated effectors. Elution positions of fractions applied to gel are indicated by *red* (in the presence of dATP) and *blue* (in the presence of ATP) arrows, respectively. d) Summary of multiple SEC experiments varying protein concentrations of NrdA (10-113 µM), NrdB (5-150 µM) and mixtures of NrdA and NrdB at ratios of 1:1 or 1:2. Molecular masses and standard deviations are calculated for 3-5 experiments, and closest estimated complex stoichiometry are shown in parenthesis, with major species underlined when appropriate (see Supplementary Fig. S2 for details).

Three-dimensional structure of *L. blandensis* NrdB

The crystal structure of the dATP-inhibited complex of *L. blandensis* NrdB at 2.45 Å resolution (PDB 5OLK) revealed a novel tetrameric arrangement hitherto not observed in the RNR family, with approximate 222 point symmetry (Fig. 6a, Supplementary Table S1). Each monomer consists of an ATP-cone domain (residues 1-103) joined by a short linker (104-106) to a metal-binding α-helical core domain (residues 107-398) and a disordered C-terminus (399-427). The latter two features are typical of the NrdB/F family. This domain arrangement gives the NrdB monomer and dimer extended conformations that are presumably flexible in solution (Fig. 6b). The dimer buries about 1100 $Å^2$ of solvent accessible area on each monomer. The tetrameric arrangement is completely dependent on interactions between the ATP cone domains, as no contacts are made between the core domains in the two dimers that make up the tetramer (Fig. 6a).

The ATP-cone domain in *L. blandensis* NrdB is structurally very similar to the one recently identified in the NrdA protein of *P. aeruginosa* (Johansson et al., 2016). The root-mean-square deviation for 92 equivalent Cα atoms is 1.2 Å. The electron density unambiguously confirms the *L. blandensis* ATP-cone's ability to bind two molecules of dATP, which it shares with *P. aeruginosa* NrdA (Fig. 6c). Despite a local sequence identity of only 31% to *P. aeruginosa* NrdA, all amino acids involved in binding both dATP molecules are conserved (Fig. 6c). The two dATP molecules bind in a "tail-to-tail" arrangement that orients the base of the "non-canonical" dATP towards the fourth, most C-terminal helix, an arrangement made possible by the binding of a Mg^{2+} ion between the triphosphate moieties.

Remarkably, the interactions between the ATP-cones in *L. blandensis* NrdB are also very similar to those seen in *P. aeruginosa* NrdA (Johansson et al., 2016), despite the fact that the ATP-cone is attached to a structurally completely different core domain. The main interactions occur between the last two helices α3 and α4 in respective ATP-cones (Fig. 6d). A hydrophobic core in *L. blandensis* NrdB involving residues Met80, Ile92 and Ile93 in both monomers is reinforced by salt bridges between residues Asp73, Asp76 in one monomer and Lys89 in the other. The two domains bury ~510 $Å^2$ of solvent accessible area. This is slightly less than the ~640 $Å^2$ buried in the equivalent interaction involving the ATP-cones of *P. aeruginosa* NrdA. Within each ATP cone, helices α3 and α4 have the same relative

304 orientation, partly determined by an internal salt bridge between the conserved Asp73 and
305 Arg95, but the helix pair in *L. blandensis* NrdB is rotated relative to its counterpart in the
306 other ATP cone by about 15° compared to *P. aeruginosa* NrdA, which reduces the number
307 of possible interactions between them. Interestingly, the dATP-induced tetramer leaves free
308 the surfaces of both dimers of *L. blandensis* NrdB that are thought to interact with the NrdA
309 subunit in productive RNR complexes, which implies that one or two dimers of *L. blandensis*
310 NrdA could attach to these surfaces in a near-productive fashion in $\alpha_2\beta_4$ or $\alpha_4\beta_4$ complexes
311 (Fig. 6a).

312 Two metal ions are found to bind to each of the monomers of *L. blandensis* NrdB.
313 Comparison of their B-factors with those of surrounding atoms suggest that they are fourth
314 row elements with close to full occupancy, but does not enable us to distinguish between
315 Mn, Fe or Ca. No metal ions were added to the protein preparation, but crystals were
316 obtained in 0.2 M $CaCl_2$. The coordination distances are long for an RNR metal center, with
317 the smallest distances being 2.3–2.4 Å. The distance between metal ions varies between
318 3.4–3.8 Å in the four monomers (Supplementary Fig. S3), but the metal coordination is very
319 similar. Interestingly, Tyr207 is found near the metal site at the position expected for a
320 radical-carrying Tyr, but it is not hydrogen-bonded to the metal site, its hydroxyl group being
321 at around 6 Å from the side chain of Glu170. Tyr207 is H-bonded to the side chain of
322 Thr294, but the latter is not H-bonded to a metal center ligand. On the other side of the metal
323 site, Trp177 is H-bonded to the side chain of Glu263. This tryptophan is completely
324 conserved in the NrdBi subclass (Supplementary Fig. S4). It makes the same interaction as
325 Trp111 from *E. coli* NrdB, despite the fact that it is projected from the first helix of the 4-helix
326 bundle containing the metal center ligands rather than the second. The first helix of the
327 bundle has a very unusual distortion in the middle (Supplementary Fig. S5). Normally this is
328 an undistorted α-helix, but in *L. blandensis* NrdB, residues 171–175 form a loop that bulges
329 away from the metal site, with the exception of Lys174, whose side chain is projected
330 towards the metal site and is H-bonded to Glu170 (Fig. 6e). The significance of this distortion
331 is at present not clear.

332 The nature of the metallo-cofactor was addressed by X-band EPR spectroscopy and
333 catalytically active samples were analyzed at 5 - 32 K. The spectra revealed a mixture of
334 signals from low and high-valent manganese species (Fig. 7a). In particular, at 5 K a 6-line
335 signal attributable to low valent Mn (Mn^{II}) was clearly visible, overlaid with a complex
336 multiline signal with a width of approximately 1250G. Increasing the temperature to 32 K
337 resulted in a significant decrease of the latter signal, while the 6-line feature remained
338 relatively intense (Fig. 7a, top and middle). The shape, width and temperature dependence
339 of the multiline signal are all highly reminiscent of the signal reported for super-oxidized
340 manganese catalase as well as the 16-line signal observed during the assembly of the
341 dimanganese/tyrosyl radical cofactor in NrdF RNR, and is attributable to a strongly coupled
342 $Mn^{III}Mn^{IV}$ dimer (S_{Total} = ½) (Fig. 7a, bottom) (Cotruvo, Stich, Britt, & Stubbe, 2013; Zheng,
343 Khangulov, Dismukes, & Barynin, 1994). The low valent species appeared to be weakly
344 bound to the protein, while the $Mn^{III}Mn^{IV}$ dimer was retained in the protein following desalting
345 (Supplementary Fig. S6). The observation of a high-valent Mn cofactor is consistent with the
346 Mn-dependent increase in catalytic activity of the enzyme and its inhibition by the addition of
347 Fe^{2+}(Fig. 7b-c), and is suggestive of a novel high-valent homodimeric Mn-cofactor. Indeed,
348 earlier calculations have shown that high-valent Mn-dimers have reduction potentials similar
349 to that of the tyrosyl radical in standard class I RNRs, but are hitherto unobserved in RNRs

(Roos & Siegbahn, 2011). A more detailed biophysical characterization of this cofactor is currently ongoing.

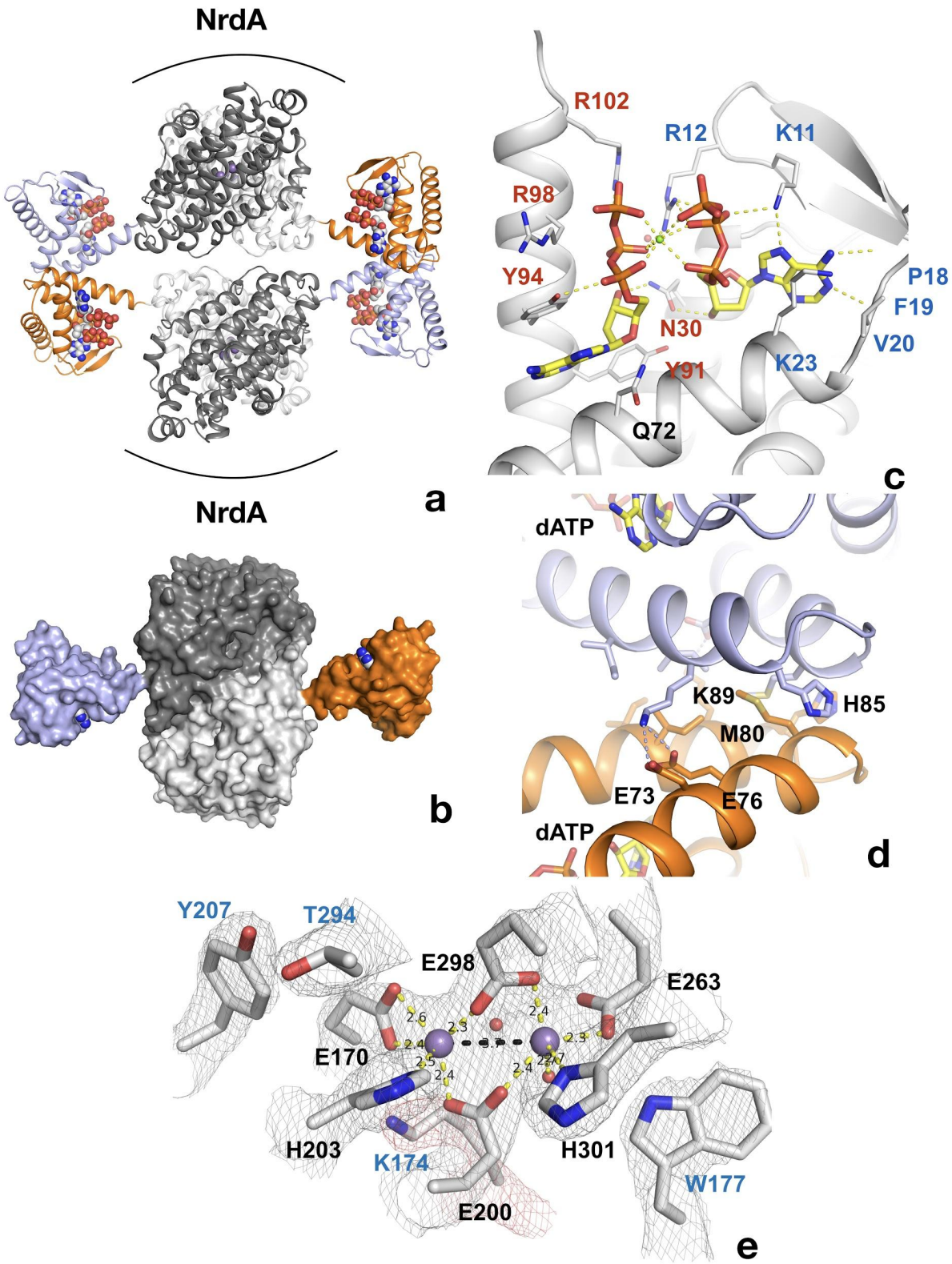

354 **Figure 6. Structure of tetrameric *L. blandensis* NrdB in complex with dATP.** a) Overall
355 structure of the NrdB tetramer. The two monomers of each dimer are colored in different
356 shades of gray, while the N-terminal ATP-cones are colored orange and light blue
357 respectively. The dATP molecules are shown in CPK representation. The curved lines at the
358 top and bottom of each dimer core indicate the proposed binding area in the active $\alpha_2\beta_2$
359 complex of RNRs. b) Surface representation of the NrdB dimer, showing the presumably
360 flexible nature of the ATP-cones in solution. The color scheme is as in panel a). c) Binding of
361 two dATP molecules to the ATP-cone. The dATP molecules are shown as sticks. Residues
362 involved in binding the two dATP molecules are labeled in blue and red respectively. Polar
363 contacts are shown as dotted yellow lines. d) The interface between ATP-cones in the NrdB
364 tetramer. Chains A and D are shown in light blue and orange respectively. Side chains of
365 residues involved in the interface are labeled. The two dATP molecules closest to the
366 interface are shown as sticks. Polar contacts are shown as yellow dotted lines. e) Structure
367 of the metal site in chain C, which is representative of the others. Metal ions are shown as
368 purple spheres. 2m|Fo|-D|Fc| electron density is shown as a grey mesh, contoured at 1.4 σ.
369 The density for Lys174 is shown in red for clarity.

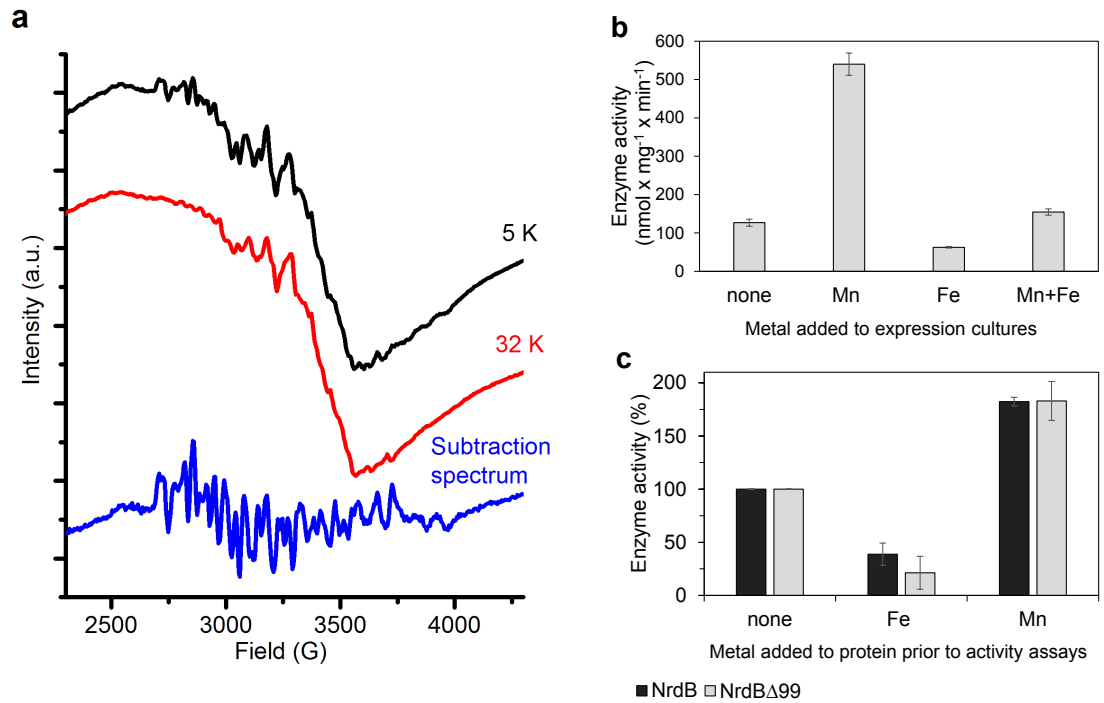

370

371

372 **Figure 7. Type of dinuclear metal center of *L. blandensis* NrdB and metal-dependency**
373 **of enzyme activity.** (a) X-band EPR spectra of catalytically active, non-reconstituted,
374 samples recorded at 5 K (*black*, top); 32 K (*red*, middle) (signal intensity multiplied by 3.7 for
375 clarity; multiline spectrum obtained by subtraction of a scaled 32K spectrum from the 5K
376 spectrum (*blue*, bottom) (signal intensity multiplied by 3 for clarity). Instrument settings:
377 microwave frequency = 9.28 GHz; power = 1 mW; modulation amplitude = 10G; modulation
378 frequency = 100 kHz. (b) Enzyme activity of NrdBΔ99 purified from heterologously
379 expressed cultures grown with addition of different divalent metal ions as indicated; the Mn-
380 sample was used for the EPR analysis. (c) Enzyme activity was measured after addition of a
381 total concentration of 20 μM divalent metal ions to 10 μM of wild-type or NrdBΔ99 protein as

382 indicated. Enzyme activity without addition of metals was set as 100% and corresponded to
383 592 and 217 nmol mg^{-1} min^{-1} for wild type and NrdBΔ99 enzymes respectively. Error bars
384 indicate the standard deviation of three measurements.

385 *L. blandensis* NrdB binds two nucleotide molecules per ATP-
386 cone

387 The finding that two dATP molecules were bound to the ATP-cone in the 3D structure
388 prompted us to investigate nucleotide binding using isothermal titration calorimetry (ITC).
389 Binding curves for dATP, ATP and dADP to NrdB, including a reverse titration of NrdB to
390 dATP, were all consistent with a single set of binding sites except for the ATP-cone deletion
391 mutant (NrdBΔ99), which did not bind nucleotides at all (Fig. 8). Using information available
392 from the 3D structure, a fixed stoichiometry of 2 was used to fit dATP binding to NrdB. The fit
393 indicated 59% active (i.e. nucleotide binding) protein. Fitting dADP and ATP with a 59%
394 proportion of active protein taken from the dATP experiment, we could calculate
395 stoichiometries of 2.2 and 2.1 for ATP and dADP respectively, indicating that each NrdB
396 monomer can bind two molecules of adenosine nucleotides (Fig. 8f). K_d for the three
397 different nucleotides (Fig. 8f) indicated a 38-fold and 15-fold lower affinity for ATP and dADP
398 compared to dATP. Thermodynamic parameters (Fig. 8f) indicated that the interactions are
399 enthalpy-driven, with negative ΔH values of -79, -44 and -103 for dATP, ATP and dADP
400 respectively.

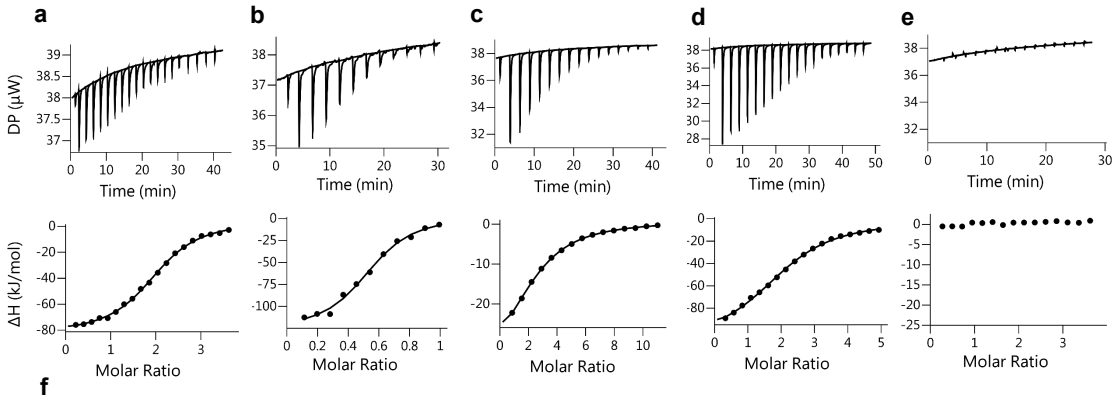

f

protein	ligand	N	K_d (µM)	ΔH (kJ mol^{-1})	ΔG (kJ mol^{-1})	-TΔS (kJ mol^{-1})
NrdB	dATP	2*	1 ± 0.2	-79 ± 10	-33	47 ± 10
NrdB	ATP	2.2 ± 0.4	38 ± 2	-44 ± 4	-24	20 ± 4
NrdB	dADP	2.1 ± 0.2	15 ± 1.5	-103 ± 9	-26	77 ± 8
NrdBΔ99	dATP	ND	ND	ND	ND	ND

401

402 **Figure 8:** Representative ITC thermograms obtained by titration of dATP (a), ATP (c) and
403 dADP (d) into NrdB. Isothermal calorimetric enthalpy changes (upper panel) and resulting
404 binding isotherms (lower panel) are shown. Reverse titration of NrdB to dATP (b). Titration of
405 dATP to NrdBΔ99 (e). Thermodynamic parameters of ligand binding to NrdB (f). Binding
406 isotherms were fitted using a one-set-of sites binding model. Values are reported as the
407 mean ± SD of three titrations (and additional two reverse titrations for dATP). All titrations

were performed at 10°C as described in Materials and Methods. *=binding stoichiometry was kept constant N=2, considering monomeric protein concentrations. ND=not detected.

Discussion

It is critically important for an organism to control the supply of dNTPs to allow fidelity in DNA replication and repair (Mathews, 2006). Specificity regulation of RNR makes sure relative concentrations of dNTPs fit the organism's DNA composition. On the other hand, activity regulation assures absolute concentrations of dNTPs follow the different requirements through the cell cycle (Hofer et al., 2012). Specificity regulation of RNRs is ubiquitous, integrated in the catalytic subunit of the enzyme, and works via the classical homooligomeric model of allosteric regulation (Andersson et al., 2000; Hofer et al., 2012; Larsson et al., 2004; Reichard, 2010; Swain & Gierasch, 2006; Torrents et al., 2000; Zimanyi et al., 2016). In contrast, the activity regulation is controlled by an accessory domain, the ATP-cone, and works by affecting the distribution of the holoenzyme heteromeric complexes. Moreover, the ATP-cone is only found in some RNRs, and appears to be gained by domain shuffling when evolutionary selection favours it and lost when selection decreases (Lundin, Berggren, Logan, & Sjöberg, 2015). These dynamics are further evidenced by the differences in mechanisms recently discovered in class I RNRs (Ando et al., 2011; Ando et al., 2016; Fairman et al., 2011; Johansson et al., 2016; Jonna et al., 2015). The current study was prompted by the interesting observation that several radical-generating subunits of the NrdBi subclass possess an N-terminal ATP-cone and that a few radical-generating subunits of the NrdF subclass possess a C-terminal ATP-cone. Our discovery evokes several pertinent questions: does the ATP-cone fused to a radical-generating subunit function as an allosteric on/off switch; how does it affect the distribution of holoenzyme complexes under active and inhibited conditions; is its structural mode of action similar to that of ATP-cones fused to the catalytic subunit?

We have delineated the function of the ATP-cone that is N-terminally fused to the *L. blandensis* NrdBi protein. In the presence of the positive effector ATP, *L. blandensis* NrdBi was a dimer, which by interaction with the *L. blandensis* catalytic subunit NrdAi formed the common active $\alpha_2\beta_2$ complex, also found in e.g. *E. coli*, *P. aeruginosa* and eukaryotic class I RNRs. Binding of dATP to the ATP-cone instead promoted oligomerization of *L. blandensis* NrdBi to an inactive β_4 complex, with a novel tetrameric structure revealed by crystallography. This oligomerization is reminiscent of the "ring-shaped" α_4 and α_6 complexes formed by dATP binding to the NrdA-linked ATP-cones in *P. aeruginosa* and eukaryotic RNRs. When *L. blandensis* NrdAi was added to the dATP-loaded NrdBi tetramer, higher molecular mass complexes of $\alpha_2\beta_4$ and $\alpha_4\beta_4$ appeared. The NrdA dimers presumably bind to the NrdB tetramers in a 'nonproductive' orientation, which does not allow efficient electron transfer between NrdA and NrdB. The crystal structure shows that the tetramerization of *L. blandensis* NrdBi leaves the putative interaction surface for NrdAi free, which is consistent with the possibility to form both $\alpha_2\beta_4$ and $\alpha_4\beta_4$ oligomers. However the structure does not suggest the structural basis for a disruption of the cysteinyl radical generation pathway in these non-productive complexes.

The structure of the dATP-loaded *L. blandensis* NrdB shows that it binds two dATP molecules per ATP-cone. Both molecules bind to the same site and interact with each other through a Mg^{2+} ion. Most allosterically regulated RNRs characterized so far bind only one

452 dATP molecule per ATP-cone. However, a novel class of ATP-cones that binds two dATP
453 molecules was recently characterized in *P. aeruginosa* NrdA (Johansson et al., 2016; Jonna
454 et al., 2015). The NrdB-linked ATP-cone of *L. blandensis* has sequence motifs characteristic
455 of this kind of ATP-cone. The structure confirms that both dATP molecules bind essentially
456 identically as in *P. aeruginosa* NrdA and that the ATP-cones make similar interactions to
457 each other, distinct from those made in the eukaryotic α_6 complexes. It has also been shown
458 in the RNR transcriptional regulator NrdR, that ATP and dATP bind with positive
459 cooperativity to its ATP-cone (McKethan & Spiro, 2013), implying binding of more than one
460 nucleotide molecule.

461 The ATP-cone in *L. blandensis* NrdBi offers a unique possibility to measure its binding
462 capacity for (deoxy)adenosine nucleotides. This has not been possible in earlier studied
463 RNRs, where the ATP-cone is bound to the α subunit that also possesses a binding site for
464 allosteric regulation of substrate specificity. ITC ligand binding studies confirmed that the *L.*
465 *blandensis* ATP-cone bound two dATP molecules, and showed that it also can bind two
466 molecules of ATP or two molecules of dADP. Structurally, binding of dADP is not surprising,
467 since the γ-phosphates of the dATP molecules make only one interaction with the protein,
468 through Arg102, and they only contribute 2 of the 6 coordinating atoms of the intervening
469 Mg^{2+} ion. Nonetheless, this is the first observation of dADP binding to the ATP-cone of an
470 RNR enzyme. dADP inhibits enzyme activity in a similar manner to dATP, but higher
471 concentrations are required. *In vivo*, deoxyribonucleoside diphosphates are rapidly
472 converted to triphosphates and cellular dADP concentrations are very low (Mathews, 2014;
473 Traut, 1994). Nevertheless, dADP is one of the products of *L. blandensis* RNR, and perhaps
474 local concentrations are higher. The ability of dADP to regulate the activity of *L. blandensis*
475 RNR may enable it to react more rapidly to changes in (deoxy)adenosine nucleotide
476 concentrations and provide the cell with a fitness advantage. Binding of deoxyadenosine di-
477 and monophosphates has been described for the ATP-cone in NrdR (Grinberg et al., 2006;
478 McKethan & Spiro, 2013).

479 Based on the variable occurrence of the ATP-cone in RNR catalytic subunits, we have
480 earlier hypothesized that its presence in RNRs is part of a dynamic process of gains and
481 losses on a relatively short evolutionary time scale (Lundin et al., 2015). This suggests that
482 the ATP-cone, contrary to what might be expected for a domain involved in allostery, does
483 not require a long evolutionary period of integration with a protein to contribute to regulation
484 and that it hence lends itself to a highly dynamic evolution of allosteric activity control
485 (Lundin et al., 2015). This hypothesis is nicely supported by the N-terminally positioned ATP-
486 cone, in the radical-generating subunit, NrdB, of *L. blandensis* RNR described here. No RNR
487 in the phylogenetic subclass NrdAi/Bi contains an ATP-cone in the catalytic subunit, and only
488 a minority – mostly encoded by Flavobacteria, a marine class of Bacteroidetes – have an
489 NrdB with an ATP-cone, suggesting the relatively recent acquisition of the ATP-cone to an
490 RNR subclass that is otherwise not activity regulated (Fig. 1). Moreover, in the Ib subclass,
491 which also lacks ATP-cones in the catalytic subunit, we detected a C-terminally positioned
492 ATP-cone in the radical-generating subunit. This was found in only two sequences from
493 closely related organisms and might hence be an example of an even more recent
494 evolutionary event.

495 The evidence we have presented here for an ATP/dATP-sensing master switch of the *L.*
496 *blandensis* NrdAi/NrdBi class I RNR, suggests a potential for the use of ATP-cones to
497 control the activity of engineered proteins. Multimeric enzymes could be inactivated through

498 sequestration of one member of an active complex, by control of dATP concentrations in the
499 reaction mixture.

500 The surprises did not end with the discovery of a functional master switch in the *L.*
501 *blandensis* NrdAi/NrdBi RNR. The active center of the radical generating subunit of class I
502 RNRs have earlier been found to consist either of an $Fe^{III}Fe^{III}$ or $Mn^{III}Mn^{III}$ pair coupled to a
503 tyrosine residue acting as long-term storage for the catalytically essential radical (Berggren,
504 Lundin, & Sjöberg, 2017; Cotruvo & Stubbe, 2012), or a $Fe^{III}Mn^{IV}$ center not coupled to an
505 amino acid radical (Griese, Srinivas, & Högbom, 2014). Although further analyses are
506 required to fully characterize the *L. blandensis* NrdBi active center, it appears to present a
507 fourth type, a high-valent $Mn^{III}Mn^{IV}$ center that lacks a suitably positioned radical storage
508 amino acid. The evolutionary flexibility displayed by the ATP-cone appears hence all but
509 equaled by the evolutionary tuning possibilities of the metal centers in the radical generating
510 subunit of class I RNR.

511 Materials and Methods

512 Cloning

513 DNA fragments encoding NrdAi (WP_009781766) and NrdBi (EAQ51288) were amplified by
514 PCR from *Leeuwenhoekiella blandensis* MED217 genomic DNA, isolated as described
515 previously (Pinhassi et al., 2006), using specific primers: NrdA: LBR1_For 5'-
516 cgagCATATGAGAGAAAACACTACCAAAC-3' and LBR1_Rev 5'-
517 gcaaGGATCCTTAAGCTTCACAGCTTACA-3'. NrdB: LBR2_For 5'-
518 cgagCATATGAGTTCACAAGAGATCAAA-3', LBR2_REV 5'-
519 gcaaGGATCCTTAAAATAAGTCGTCGCTG-3', The PCR products were purified, cleaved
520 with NdeI and BamHI restriction enzymes and inserted into a pET-28a(+) expression vector
521 (Novagen, Madison, Wisconsin, USA). The obtained constructs pET-*nrdA* and pET-*nrdB*
522 contained an N-terminal hexahistidine (His) tag and thrombin cleavage site. To construct a
523 truncated NrdB mutant, lacking the entire ATP-cone domain, new forward primer
524 LBR2Δ99_For 5'-cgatCATATGCTGGAGCGTAAAACAAAT-3' was used with LBR2_REV to
525 yield a pET-*nrdB*Δ99. The cloning process and the resulting construct was similar to that of
526 the wild type protein, except that it lacked sequence coding for the N-terminal 99 amino
527 acids.

528 Protein expression

529 Overnight cultures of *E. coli* BL21(DE3)/pET28a(+) bearing pET-*nrdA*, pET-*nrdB* and pET-
530 *nrdB*Δ99 were diluted to an absorbance at 600 nm of 0.1 in LB (Luria-Bertani) liquid medium,
531 containing kanamycin (50 µg/ml) and shaken vigorously at 37°C. At an absorbance at 600
532 nm of 0.8, isopropyl-β-D-thiogalactopyranoside (Sigma) was added to a final concentration
533 of 0.01 mM for NrdA expression and 0.5 mM for NrdB and NrdBΔ99 expression. For
534 particular experiments, 0.5 mM $MnSO_4$ or 0.5 mM $FeNH_4(SO4)_2$ or the combination of both
535 metals (0.4 mM and 0.25 mM respectively) were added to NrdBΔ99 cultures. The cells were
536 grown overnight at 14°C for NrdA expression and 20°C for NrdB and NrdBΔ99 expression
537 and harvested by centrifugation.

538 # Protein purification

539 The cell pellet was resuspended in lysis buffer: 50 mM Tris-HCl pH 7.6 containing 300 mM
540 NaCl, 20% glycerol, 10 mM imidazole, 1 mM PMSF. Cells were disrupted by high pressure
541 homogenization and the lysate was centrifuged at 18,000 × g for 45 min at 4°C. The
542 recombinant His-tagged protein was first isolated by metal-chelate affinity chromatography
543 using ÄKTA prime system (GE Healthcare): the supernatant was loaded on a HisTrap FF Ni
544 Sepharose column (GE Healthcare), equilibrated with lysis buffer (w/o PMSF), washed
545 thoroughly with buffer and eluted with buffer containing 500 mM imidazole. Further
546 purification was accomplished by fast protein liquid chromatography (FPLC) on a 125 ml
547 column packed with Superose 12 Prep Grade or HiLoad 16/600 Superdex 200 pg column
548 (GE Healthcare) using ÄKTA prime system, equilibrated with buffer containing 50 mM Tris-
549 HCl pH 7.6, 300 mM NaCl, 10-20% glycerol. Eluted protein was collected. In the case of
550 NrdA, all purification steps were performed in the presence of 2 mM DTT. Protein
551 concentration was determined by measuring the UV absorbance at 280 nm based on protein
552 theoretical extinction coefficients 91,135, 46,870 and 39,420 M^{-1} cm^{-1} for NrdA, NrdB and
553 NrdB∆99 respectively. Proteins were concentrated using Amicon Ultra-15 centrifugal filter
554 units (Millipore), frozen in liquid nitrogen and stored at -80°C until used.

555 For crystallization, NrdB was subsequently cleaved by thrombin (Novagen) to remove the
556 hexahistidine tag. 41 mg NrdB was incubated with 25 U thrombin at 6°C for 3 hours, in a
557 buffer containing 40 mM Tris-HCl pH 8.4, 150 mM NaCl, and 2.5 mM $CaCl_2$ in a total volume
558 of 50 ml. Subsequently, imidazole to a final concentration of 20 mM was added and the
559 reaction mixture was applied to a HisTrap FF Ni Sepharose column in a buffer containing 20
560 mM imidazole. Unbound protein was collected, concentrated and further purified by FPLC
561 (see above) in a buffer containing Tris-HCl pH 7.6, 300 mM NaCl, and 10% glycerol. The
562 thrombin-cleaved NrdB contained three additional residues (GlySerHis) that originated from
563 the cleavage site of the enzyme at its N-terminus. Protein purity was evaluated by SDS–
564 PAGE (12%) stained with Coomassie Brilliant Blue.

565 For EPR measurements, NrdB∆99 was frozen in liquid nitrogen in EPR tubes directly after
566 imidazole elution from the HisTrap column. Additional EPR samples were frozen after
567 desalting the protein using PD-10 desalting columns (GE Healthcare).

568 # Enzyme activity assays

569 Enzyme assays were performed at room temperature in 50 mM Tris-HCl at pH 8 in volumes
570 of 50 µl. Reaction conditions, giving maximal activity were determined experimentally. In a
571 standard reaction the constituents were; 10 mM DTT, 10 mM MgAc, 10 mM KCl, 0.8 mM (or
572 when indicated 3 mM) CDP, and various concentrations of allosteric effectors ATP, dATP or
573 dADP. Mixtures of 0.5 µM NrdA and 2 µM wild type NrdB or NrdB∆99 (for determination of s-
574 site K_L) (Fig. 3a-b) or 0.5 µM of NrdB and 2 uM NrdA (for determination of a-site K_L), (Fig. 3
575 c-f) were used. Some components were explicitly varied in specific experiments. Generally,
576 0.8 mM CDP was used as substrate. High CDP concentration (3 mM) was used for dADP
577 titrations, to exclude potential product inhibition by binding of dADP to the active site. When
578 dTTP was used as an s-site effector, 0.5 mM or 0.8 mM GDP was used as substrate. In four
579 substrate assays, the four substrates CDP, ADP, GDP and UDP were simultaneously
580 present in the mixture at concentrations of 0.5 mM each. The substrate mixture was added

581 last to start the reactions. Certain assays were performed in the presence of $Mn(CH_3COO)_2$
582 or $FeNH_4(SO4)$: 20 µM of the indicated metal was added to 10 µM NrdB or NrdB∆99 protein,
583 incubated for 10 minutes, mixed with NrdA and added to the reaction mixture.

584 Enzyme reactions were incubated for 10-30 minutes and then stopped by the addition of
585 methanol. The chosen incubation time gave a maximum substrate turnover of 30%.
586 Substrate conversion was analyzed by HPLC using a Waters Symmetry C18 column (150 ×
587 4.6 mm, 3.5 µm pore size) equilibrated with buffer A. 25 µl samples were injected and eluted
588 at 1 ml/min with a linear gradient of 0–100% buffer B (buffer A: 10% methanol in 50 mM
589 potassium phosphate buffer, pH 7.0, supplemented with 10 mM tributylammonium
590 hydroxide; buffer B: 30% methanol in 50 mM potassium phosphate buffer, pH 7.0,
591 supplemented with 10 mM tributylammonium hydroxide). Compound identification was
592 achieved by comparison with injected standards. Relative quantification was obtained by
593 peak height measurements in the chromatogram (UV absorbance at 271 nm) in relation to
594 standards. Specific activities of either NrdA (Fig. 2 a-b) or NrdB (Fig. 2 c-f) were determined.
595 Specific activities varied between protein preparations. In some cases the data was
596 standardized to activity percent, where 100% was determined as maximum enzyme activity
597 in a specific condition.

598 From a direct plot of activity versus concentration of effector, the K_L values for binding of
599 effectors to the s-site and the a-site, were calculated in SigmaPlot using the equation:

600 $v = V_{max} \times [dNTP] / (K_L + [dNTP])$

601 and K_i for non-competitive dATP inhibition at NrdB was calculated in Sigmaplot using the
602 equation:

603 $v = V_{max} / (1 + ([dNTP]/K_i)$

604 GEMMA analysis

605 In GEMMA, biomolecules are electrosprayed into gas phase, neutralized to singly charged
606 particles, and the gas phase electrophoretic mobility is measured with a differential mobility
607 analyzer. The mobility of an analyzed particle is proportional to its diameter, which therefore
608 allows for quantitative analysis of the different particle sizes contained in a sample
609 (Kaufman, Skogen, Dorman, Zarrin, & Lewis, 1996). The GEMMA instrumental setup and
610 general procedures were as described previously (Rofougaran et al., 2008). NrdA, NrdB and
611 NrdB∆99 proteins were equilibrated by Sephadex G-25 chromatography into a buffer
612 containing 100 mM ammonium acetate, pH 7.8. In addition, 2 mM DTT was added to the
613 NrdA protein solutions to increase protein stability. Prior to GEMMA analysis, the protein
614 samples were diluted to a concentration of 0.025–0.1 mg/ml in a buffer containing 20 mM
615 ammonium acetate, pH 7.5, 0.005% (v/v) Tween 20, nucleotides (when indicated), and
616 magnesium acetate (equimolar to the total nucleotide concentration), incubated for 5 min at
617 room temperature, centrifuged and applied to the GEMMA instrument. Protein
618 concentrations higher than normally recommended for GEMMA were needed to see the
619 larger oligomeric complexes and the experiments to measure NrdA-NrdB interactions were
620 run at as low flow rate as possible (driven by 1.4 Psi pressure) to minimize false interactions
621 that may appear with elevated protein concentration if the flow-rate recommended by the

622 manufacturer is used (3.7 Psi). The lower flow-rates give less sensitivity, though, and a flow
623 rate driven by 2 Psi was sufficient to prevent in most experiments.

624 Analytical size exclusion chromatography

625 Fast protein liquid chromatography on a Superdex 200 PC 3.2/30 column (with a total
626 volume of 2.4 ml) and ÄKTA prime system (GE Healthcare) was performed. The column was
627 equilibrated with SEC buffer containing 50 mM Tris-HCl pH 8, 50 mM KCl, 10% glycerol, 10
628 mM magnesium acetate, 2 mM DTT and when applicable either 3 mM ATP or 0.1-0.5 mM
629 dATP. 50 µL samples containing NrdA, NrdB or both subunits in the presence or the
630 absence of indicated amounts of nucleotides, were incubated for 10 minutes in room
631 temperature, centrifuged and applied to the column with a flow rate of 0.07 ml/min. When
632 nucleotides were added to proteins, they were also included in the buffer at the same
633 concentration to avoid dissociation of nucleotide-induced protein complexes during the run.
634 Varying concentrations of proteins were used in the range of 10-113 µM and 5-150 µM for
635 NrdA and NrdB respectively. For complex formation, 10-20 µM NrdA and 10-40 µM NrdB
636 were used in ratios of 1:1 or 1:2. Representative SEC chromatograms in which 20 µM NrdA,
637 20 µM NrdB or a mixture of 25 µM and 50 µM NrdA and NrdB respectively are shown in Fig.
638 5. Molecular weight was estimated based on a calibration curve, derived from globular
639 protein standards using high molecular weight SEC marker kit (GE Healthcare). Standard
640 deviations were calculated from at least 3 SEC experiments.

641 EPR measurements

642 Measurements were performed on a Bruker ELEXYS E500 spectrometer using an ER049X
643 SuperX microwave bridge in a Bruker SHQ0601 cavity equipped with an Oxford Instruments
644 continuous flow cryostat and using an ITC 503 temperature controller (Oxford Instruments).
645 Measurement temperatures ranged from 5 to 32 K, using liquid helium as coolant. The
646 spectrometer was controlled by the Xepr software package (Bruker).

647 Bioinformatics

648 RNR protein sequences were collected and scored using HMMER (Eddy, 2011) HMM
649 profiles in the RNRdb (http://rnrdb.pfitmap.org). ATP-cones were identified with the Pfam
650 ATP-cone HMM profile: PF03477. Sequences representing the diversity of NrdB were
651 selected by clustering all NrdB sequences from RefSeq at an identity threshold of 70% using
652 VSEARCH (Rognes, Flouri, Nichols, Quince, & Mahe, 2016). Sequences were aligned with
653 ProbCons (Do, Mahabhashyam, Brudno, & Batzoglou, 2005) and reliable positions for
654 phylogenetic reconstruction were manually selected. A maximum likelihood phylogeny was
655 estimated with FastTree 2 (Price, Dehal, & Arkin, 2010).

656 Isothermal titration calorimetry (ITC) measurements

657 Isothermal titration calorimetry (ITC) experiments were carried out on a MicroCal PEAQ-ITC
658 system (Malvern Instruments Ltd) in a buffer containing 25 mM HEPES (pH 7.65), 150 mM
659 NaCl, and 10% glycerol, 2 mM tris(2-carboxyethyl)phosphine, and 5 mM $MgCl_2$.
660 Measurements were done at 10°C. The initial injection volume was 0.4 µl over a duration of
661 0.8 s. All subsequent injection volumes were 2-2.5 µl over 4-5 s with a spacing of 150 s
662 between the injections. Data for the initial injection were not considered. For dATP binding

663 analysis, the concentration of NrdB in the cell was 12 μM and dATP in syringe 120 or 140
664 μM. Reverse titrations were performed with 113 μM NrdB in the syringe and 12 or 30 μM
665 dATP in the cell. For titration of dATP into NrdB∆99, protein concentration in the cell and
666 dATP concentration in the syringe were 50 μM and 900 μM respectively. For dADP binding
667 analysis, the NrdB concentration in the cell was 20-50 μM and ligand concentrations in the
668 syringe were 500-750 μM. For titration of ATP into NrdB, cell and syringe concentrations
669 were 50 and 1600 μM respectively. The data were analyzed using the built-in one set of
670 sites model of the MicroCal PEAQ-ITC Analysis Software (Malvern Instruments Ltd). A fixed
671 ligand/protein stoichiometry of 2 was used for dATP to NrdB titrations. Standard deviations in
672 thermodynamic parameters, N and K_d were estimated from the fits of three different
673 titrations.

674 Crystallization and data collection

675 The purified NrdB, digested by thrombin to remove the hexahistidine tag (see above), was
676 used for crystallization. The protein at a concentration of 9.6 mg/ml was mixed with 20 mM
677 $MgCl_2$, 2 mM TCEP and 5 mM dATP, incubated for 30 minutes and used for setting up drops
678 using commercially available screens. An initial crystal hit was obtained by the sitting drop
679 vapor diffusion method with a protein to reservoir volume ratio of 200:200 nL and incubated
680 with a 45 μl reservoir in a Triple Drop UV Polymer Plate (Molecular Dimensions, UK). A
681 Mosquito nanoliter pipetting robot (TTP Labtech, UK) was used to set up drops, which were
682 imaged by the Minstrel HT UV imaging system (Rigaku Corporation, USA) available at the
683 Lund Protein Production Platform (LP3). Crystals were obtained with a reservoir containing
684 0.2 M $CaCl_2$, 0.1 M Tris pH 8.0 and 20% w/v PEG 600 (condition #57 of the PACT screen).
685 The crystals were then further optimized using an additive screen (Hampton Research, USA)
686 and diffraction quality crystals were obtained within 1 week from a crystallization solution
687 containing an additional 3% 6-aminohexanoic acid. Crystals were picked up directly from the
688 drop without cryoprotectant and data were collected at 100 K using the ID23-1 beamline at
689 the ESRF, Grenoble, France.

690 Structure determination and model building

691 The diffraction images were integrated using the program XDS (Kabsch, 2010) and scaled
692 using the program Aimless (Evans & Murshudov, 2013) from the CCP4 package (Winn et
693 al., 2011). The structure was solved by molecular replacement (MR) in two steps, using
694 Phaser (McCoy et al., 2007). First the structure of NrdB∆99 was solved to 1.7 Å resolution
695 using the most homologous structure in the PDB, that of NrdF from *Chlamydia trachomatis*
696 (1SYY) (Högbom et al., 2004). This structure was rebuilt manually in Coot (Emsley,
697 Lohkamp, Scott, & Cowtan, 2010) and using Buccaneer (Cowtan, 2006) then refined to
698 convergence using Refmac5 (Murshudov, Vagin, & Dodson, 1997) and Buster (Bricogne,
699 2016). Full details of this structure will be presented elsewhere. In the second step, a multi-
700 body molecular replacement search was carried out using four copies of NrdB∆99 and four
701 copies of the ATP-cone from *P. aeruginosa* NrdA (Johansson et al., 2016) prepared by side
702 chain truncation using Chainsaw (Stein, 2008). A single solution was found in which all 8
703 bodies were placed, with a translation function Z score (TFZ) of 12.2. After rearrangement of
704 the ATP-cones from the MR solution to the N-termini of their respective core domains, the

structure was refined using Refmac5. Some autobuilding was performed using Buccaneer and manual rebuilding in Coot. Final refinement was done using Buster (Bricogne, 2016).

Automatically-generated non-crystallographic symmetry restraints were used. Geometry was validated using the MolProbity server (Chen et al., 2010).

Acknowledgements

We want to thank Jarone Pinhassi and Sabina Arnautovic, Linneaus University, Kalmar, Sweden, for the kind gift of *Leeuwenhoekiella blandensis* DNA, Yuliya Leontyeva, Jan-Olov Persson and Rolf Sundberg, Department of Mathematics, Stockholm University, Sweden, for excellent statistical analysis of ligand binding, Eva Muñoz and Angel Piñeiro, AFFINImeter, Santiago de Compostela, Spain for valuable assistance with analysis of ITC titrations, Hanna Jankevics Jones and John Stenson, Malvern Instruments Ltd, Malvern, UK for highly appreciated help with protein biophysical characterization and Fredrik Tholander, Karolinska Institute, Stockholm, Sweden, for generously providing his HPLC instrument for the enzyme assays. We thank the crystallization facility at Lund Protein Production Platform for crystallization trials and staff at EMBL Hamburg and ESRF beamlines for assistance with data collection. This study was supported by grants from the Swedish Cancer Society (CAN 2016/670 to BMS), the Swedish Research Council (2016-01920 to BMS, 2016-04855 to DTL), the Wenner-Gren Foundations (to BMS) and the Carl Trygger Foundation (to AH). Work in the laboratory of GB is supported by the Swedish Research Council (621-2014-5670), the Swedish Research Council for Environment, Agricultural Sciences and Spatial Planning (213-2014-880) and the European Research Council (714102).

Accession codes

References accessions from Protein Data Bank: 5OLK

Author contributions

IRG, DL, IB, NM, GB, AH, DTL and BMS designed and analyzed experiments. IRG, DL, MH, VRJ, GB, AH and DTL performed experiments. MC, CL and MS helped with setting up activity assays. All authors contributed to the final manuscript.

References

Ahmad, M. F., & Dealwis, C. G. (2013). The structural basis for the allosteric regulation of ribonucleotide reductase. *Prog Mol Biol Transl Sci, 117*, 389-410. doi:10.1016/b978-0-12-386931-9.00014-3

Andersson, J., Westman, M., Hofer, A., & Sjöberg, B. M. (2000). Allosteric regulation of the class III anaerobic ribonucleotide reductase from bacteriophage T4. *J Biol Chem, 275*(26), 19443-19448. doi:10.1074/jbc.M001490200

Ando, N., Brignole, E. J., Zimanyi, C. M., Funk, M. A., Yokoyama, K., Asturias, F. J., . . . Drennan, C. L. (2011). Structural interconversions modulate activity of Escherichia coli ribonucleotide reductase. *Proc Natl Acad Sci U S A, 108*(52), 21046-21051. doi:10.1073/pnas.1112715108

Ando, N., Li, H., Brignole, E. J., Thompson, S., McLaughlin, M. I., Page, J. E., . . . Drennan, C. L. (2016). Allosteric inhibition of human ribonucleotide reductase by dATP entails the stabilization of a hexamer. *Biochemistry, 55*(2), 373-381. doi:10.1021/acs.biochem.5b01207

Aravind, L., Wolf, Y. I., & Koonin, E. V. (2000). The ATP-cone: an evolutionarily mobile, ATP-binding regulatory domain. *J Mol Microbiol Biotechnol, 2*(2), 191-194.

Aye, Y., & Stubbe, J. (2011). Clofarabine 5'-di and -triphosphates inhibit human ribonucleotide reductase by altering the quaternary structure of its large subunit. *Proc Natl Acad Sci U S A, 108*(24), 9815-9820. doi:10.1073/pnas.1013274108

Berggren, G., Lundin, D., & Sjöberg, B.-M. (2017). Homo- and heterometallic dinuclear manganese proteins: active site assembly. In M. K. Johnson & R. A. Scott (Eds.), *Metalloprotein Active Site Assembly*: John Wiley & Sons, Ltd.

Bochner, B. R., & Ames, B. N. (1982). Complete analysis of cellular nucleotides by two-dimensional thin layer chromatography. *J Biol Chem, 257*(16), 9759-9769.

Bricogne, G. B., E.; Brandl, M.; Flensburg, C.; Keller, P.; Paciorek, W.; Roversi, P.; Sharff, A.; Smart, O.S.; Vonrhein, C.; Womack, T.O. (2016). BUSTER version 2.10.2. *Cambridge, United Kingdom: Global Phasing Ltd.*

Brown, N. C., & Reichard, P. (1969). Role of effector binding in allosteric control of ribonucleoside diphosphate reductase. *J Mol Biol, 46*(1), 39-55. doi:0022-2836(69)90056-4 [pii]

Buckstein, M. H., He, J., & Rubin, H. (2008). Characterization of nucleotide pools as a function of physiological state in Escherichia coli. *J Bacteriol, 190*(2), 718-726. doi:10.1128/jb.01020-07

Chen, V. B., Arendall, W. B., 3rd, Headd, J. J., Keedy, D. A., Immormino, R. M., Kapral, G. J., . . . Richardson, D. C. (2010). MolProbity: all-atom structure validation for macromolecular crystallography. *Acta Crystallogr D Biol Crystallogr, 66*(Pt 1), 12-21. doi:10.1107/s0907444909042073

Cotruvo, J. A., Jr., Stich, T. A., Britt, R. D., & Stubbe, J. (2013). Mechanism of assembly of the dimanganese-tyrosyl radical cofactor of class Ib ribonucleotide reductase: enzymatic generation of superoxide is required for tyrosine oxidation via a Mn(III)Mn(IV) intermediate. *J Am Chem Soc, 135*(10), 4027-4039. doi:10.1021/ja312457t

Cotruvo, J. A., Jr., & Stubbe, J. (2012). Metallation and mismetallation of iron and manganese proteins in vitro and in vivo: the class I ribonucleotide reductases as a case study. *Metallomics, 4*(10), 1020-1036. doi:10.1039/c2mt20142a

Cowtan, K. (2006). The Buccaneer software for automated model building. 1. Tracing protein chains. *Acta Crystallogr D Biol Crystallogr, 62*(Pt 9), 1002-1011. doi:10.1107/s0907444906022116

Crona, M., Avesson, L., Sahlin, M., Lundin, D., Hinas, A., Klose, R., . . . Sjöberg, B. M. (2013). A rare combination of ribonucleotide reductases in the social amoeba Dictyostelium discoideum. *J Biol Chem, 288*(12), 8198-8208. doi:10.1074/jbc.M112.442434

Do, C. B., Mahabhashyam, M. S. P., Brudno, M., & Batzoglou, S. (2005). ProbCons: Probabilistic consistency-based multiple sequence alignment. *Genome Research, 15*(2), 330-340. doi:10.1101/gr.2821705

Eddy, S. R. (2011). Accelerated profile HMM searches. *PLoS Comput Biol, 7*(10), e1002195. doi:10.1371/journal.pcbi.1002195

Emsley, P., Lohkamp, B., Scott, W. G., & Cowtan, K. (2010). Features and development of Coot. *Acta Crystallogr D Biol Crystallogr, 66*(Pt 4), 486-501. doi:10.1107/s0907444910007493

Eriksson, M., Uhlin, U., Ramaswamy, S., Ekberg, M., Regnström, K., Sjöberg, B. M., & Eklund, H. (1997). Binding of allosteric effectors to ribonucleotide reductase protein R1: reduction of active-site cysteines promotes substrate binding. *Structure, 5*(8), 1077-1092.

797 Evans, P. R., & Murshudov, G. N. (2013). How good are my data and what is the resolution?
798 *Acta Crystallogr D Biol Crystallogr, 69*(Pt 7), 1204-1214.
799 doi:10.1107/s0907444913000061
800 Fairman, J. W., Wijerathna, S. R., Ahmad, M. F., Xu, H., Nakano, R., Jha, S., . . . Dealwis, C.
801 G. (2011). Structural basis for allosteric regulation of human ribonucleotide reductase
802 by nucleotide-induced oligomerization. *Nat Struct Mol Biol, 18*(3), 316-322.
803 doi:nsmb.2007 [pii]10.1038/nsmb.2007
804 Fernandez-Gomez, B., Richter, M., Schuler, M., Pinhassi, J., Acinas, S. G., Gonzalez, J. M.,
805 & Pedros-Alio, C. (2013). Ecology of marine Bacteroidetes: a comparative genomics
806 approach. *ISME J, 7*(5), 1026-1037. doi:10.1038/ismej.2012.169
807 Griese, J. J., Srinivas, V., & Högbom, M. (2014). Assembly of nonheme Mn/Fe active sites in
808 heterodinuclear metalloproteins. *J Biol Inorg Chem, 19*(6), 759-774.
809 doi:10.1007/s00775-014-1140-7
810 Grinberg, I., Shteinberg, T., Gorovitz, B., Aharonowitz, Y., Cohen, G., & Borovok, I. (2006).
811 The Streptomyces NrdR transcriptional regulator is a Zn ribbon/ATP cone protein that
812 binds to the promoter regions of class Ia and class II ribonucleotide reductase
813 operons. *J Bacteriol, 188*(21), 7635-7644. doi:JB.00903-06 [pii]10.1128/JB.00903-06
814 Gunasekaran, K., Ma, B., & Nussinov, R. (2004). Is allostery an intrinsic property of all
815 dynamic proteins? *Proteins, 57*(3), 433-443. doi:10.1002/prot.20232
816 Hofer, A., Crona, M., Logan, D. T., & Sjöberg, B. M. (2012). DNA building blocks: keeping
817 control of manufacture. *Crit Rev Biochem Mol Biol, 47*(1), 50-63.
818 doi:10.3109/10409238.2011.630372
819 Huang, M., Parker, M. J., & Stubbe, J. (2014). Choosing the right metal: case studies of
820 class I ribonucleotide reductases. *J Biol Chem, 289*(41), 28104-28111.
821 doi:10.1074/jbc.R114.596684
822 Högbom, M., Stenmark, P., Voevodskaya, N., McClarty, G., Gräslund, A., & Nordlund, P.
823 (2004). The radical site in chlamydial ribonucleotide reductase defines a new R2
824 subclass. *Science, 305*(5681), 245-248. doi:10.1126/science.1098419
825 Johansson, R., Jonna, V. R., Kumar, R., Nayeri, N., Lundin, D., Sjöberg, B. M., . . . Logan,
826 D. T. (2016). Structural mechanism of allosteric activity regulation in a ribonucleotide
827 reductase with double ATP cones. *Structure, 24*(6), 906-917.
828 doi:10.1016/j.str.2016.03.025
829 Jonna, V. R., Crona, M., Rofougaran, R., Lundin, D., Johansson, S., Brännström, K., . . .
830 Hofer, A. (2015). Diversity in overall activity regulation of ribonucleotide reductase. *J*
831 *Biol Chem, 290*(28), 17339-17348. doi:10.1074/jbc.M115.649624
832 Kabsch, W. (2010). XDS. *Acta Crystallogr D Biol Crystallogr, 66*(Pt 2), 125-132.
833 doi:10.1107/s0907444909047337
834 Kashlan, O. B., Scott, C. P., Lear, J. D., & Cooperman, B. S. (2002). A comprehensive
835 model for the allosteric regulation of mammalian ribonucleotide reductase. Functional
836 consequences of ATP- and dATP-induced oligomerization of the large subunit.
837 *Biochemistry, 41*(2), 462-474. doi:10.1021/bi011653a
838 Kaufman, S. L., Skogen, J. W., Dorman, F. D., Zarrin, F., & Lewis, K. C. (1996).
839 Macromolecule analysis based on electrophoretic mobility in air: globular proteins.
840 *Anal Chem, 68*(11), 1895-1904. doi:10.1021/ac951128f
841 Kumar, D., Abdulovic, A. L., Viberg, J., Nilsson, A. K., Kunkel, T. A., & Chabes, A. (2011).
842 Mechanisms of mutagenesis in vivo due to imbalanced dNTP pools. *Nucleic Acids*
843 *Res, 39*(4), 1360-1371. doi:10.1093/nar/gkq829
844 Larsson, K. M., Jordan, A., Eliasson, R., Reichard, P., Logan, D. T., & Nordlund, P. (2004).
845 Structural mechanism of allosteric substrate specificity regulation in a ribonucleotide
846 reductase. *Nat Struct Mol Biol, 11*(11), 1142-1149. doi:10.1038/nsmb838
847 Lundin, D., Berggren, G., Logan, D. T., & Sjöberg, B. M. (2015). The origin and evolution of
848 ribonucleotide reduction. *Life (Basel), 5*(1), 604-636. doi:10.3390/life5010604
849 Mathews, C. K. (2006). DNA precursor metabolism and genomic stability. *FASEB J, 20*(9),
850 1300-1314. doi:20/9/1300 [pii]10.1096/fj.06-5730rev

Mathews, C. K. (2014). Deoxyribonucleotides as genetic and metabolic regulators. *FASEB J, 28*(9), 3832-3840. doi:10.1096/fj.14-251249

McCoy, A. J., Grosse-Kunstleve, R. W., Adams, P. D., Winn, M. D., Storoni, L. C., & Read, R. J. (2007). Phaser crystallographic software. *J Appl Crystallogr, 40*(Pt 4), 658-674. doi:10.1107/s0021889807021206

McKethan, B. L., & Spiro, S. (2013). Cooperative and allosterically controlled nucleotide binding regulates the DNA binding activity of NrdR. *Mol Microbiol, 90*(2), 278-289. doi:10.1111/mmi.12364

Murshudov, G. N., Vagin, A. A., & Dodson, E. J. (1997). Refinement of macromolecular structures by the maximum-likelihood method. *Acta Crystallogr D Biol Crystallogr, 53*(Pt 3), 240-255. doi:10.1107/s0907444996012255

Nordlund, P., & Reichard, P. (2006). Ribonucleotide reductases. *Annu Rev Biochem, 75*, 681-706. doi:10.1146/annurev.biochem.75.103004.142443

Nussinov, R., & Tsai, C. J. (2013). Allostery in disease and in drug discovery. *Cell, 153*(2), 293-305. doi:10.1016/j.cell.2013.03.034

Pai, C. C., & Kearsey, S. E. (2017). A critical balance: dNTPs and the maintenance of genome stability. *Genes (Basel), 8*(2). doi:10.3390/genes8020057

Pinhassi, J., Bowman, J. P., Nedashkovskaya, O. I., Lekunberri, I., Gomez-Consarnau, L., & Pedros-Alio, C. (2006). Leeuwenhoekiella blandensis sp. nov., a genome-sequenced marine member of the family Flavobacteriaceae. *Int J Syst Evol Microbiol, 56*(Pt 7), 1489-1493. doi:10.1099/ijs.0.64232-0

Price, M. N., Dehal, P. S., & Arkin, A. P. (2010). FastTree 2 – approximately maximum-likelihood trees for large alignments. *PLoS One, 5*(3), e9490. doi:10.1371/journal.pone.0009490

Reichard, P. (2010). Ribonucleotide reductases: substrate specificity by allostery. *Biochem Biophys Res Commun, 396*(1), 19-23. doi:10.1016/j.bbrc.2010.02.108

Rofougaran, R., Crona, M., Vodnala, M., Sjöberg, B.-M., & Hofer, A. (2008). Oligomerization status directs overall activity regulation of the Escherichia coli class Ia ribonucleotide reductase. *J Biol Chem, 283*(51), 35310-35318. doi:10.1074/jbc.M806738200

Rofougaran, R., Vodnala, M., & Hofer, A. (2006). Enzymatically active mammalian ribonucleotide reductase exists primarily as an alpha6beta2 octamer. *J Biol Chem, 281*(38), 27705-27711. doi:M605573200 [pii]10.1074/jbc.M605573200

Rognes, T., Flouri, T., Nichols, B., Quince, C., & Mahe, F. (2016). VSEARCH: a versatile open source tool for metagenomics. *PeerJ, 4*, e2584. doi:10.7717/peerj.2584

Roos, K., & Siegbahn, P. E. (2011). Oxygen cleavage with manganese and iron in ribonucleotide reductase from Chlamydia trachomatis. *J Biol Inorg Chem, 16*(4), 553-565. doi:10.1007/s00775-011-0755-1

Stein, N. (2008). CHAINSAW: a program for mutating pdb files used as templates in molecular replacement. *J Appl Cryst, 41*, 641-643.

Swain, J. F., & Gierasch, L. M. (2006). The changing landscape of protein allostery. *Curr Opin Struct Biol, 16*(1), 102-108. doi:10.1016/j.sbi.2006.01.003

Thelander, L., & Reichard, P. (1979). Reduction of ribonucleotides. *Annu Rev Biochem, 48*, 133-158. doi:10.1146/annurev.bi.48.070179.001025

Torrents, E. (2014). Ribonucleotide reductases: essential enzymes for bacterial life. *Front Cell Infect Microbiol, 4*, 52. doi:10.3389/fcimb.2014.00052

Torrents, E., Buist, G., Liu, A., Eliasson, R., Kok, J., Gibert, I., . . . Reichard, P. (2000). The anaerobic (class III) ribonucleotide reductase from Lactococcus lactis. Catalytic properties and allosteric regulation of the pure enzyme system. *J Biol Chem, 275*(4), 2463-2471.

Torrents, E., Westman, M., Sahlin, M., & Sjöberg, B. M. (2006). Ribonucleotide reductase modularity: atypical duplication of the ATP-cone domain in Pseudomonas aeruginosa. *J Biol Chem, 281*(35), 25287-25296. doi:M601794200 [pii]10.1074/jbc.M601794200

Traut, T. W. (1994). Physiological concentrations of purines and pyrimidines. *Mol Cell Biochem, 140*(1), 1-22.

906 Watt, D. L., Buckland, R. J., Lujan, S. A., Kunkel, T. A., & Chabes, A. (2016). Genome-wide
907 analysis of the specificity and mechanisms of replication infidelity driven by
908 imbalanced dNTP pools. *Nucleic Acids Res, 44*(4), 1669-1680.
909 doi:10.1093/nar/gkv1298
910 Winn, M. D., Ballard, C. C., Cowtan, K. D., Dodson, E. J., Emsley, P., Evans, P. R., . . .
911 Wilson, K. S. (2011). Overview of the CCP4 suite and current developments. *Acta*
912 *Crystallogr D Biol Crystallogr, 67*(Pt 4), 235-242. doi:10.1107/s0907444910045749
913 Zheng, M., Khangulov, S. V., Dismukes, G. C., & Barynin, V. V. (1994). Electronic structure
914 of dimanganese(II,III) and dimanganese(III,IV) complexes and dimanganese catalase
915 enzyme - a general EPR spectral simulation approach. *Inorg Chem, 33*(2), 382-387.
916 doi:10.1021/ic00080a030
917 Zimanyi, C. M., Chen, P. Y., Kang, G., Funk, M. A., & Drennan, C. L. (2016). Molecular basis
918 for allosteric specificity regulation in class Ia ribonucleotide reductase from
919 Escherichia coli. *Elife, 5*, e07141. doi:10.7554/eLife.07141

920